BIOMATERIALS

A reversible thermoresponsive sealant for temporary closure of ocular trauma

Niki Bayat,[1] Yi Zhang,[2,3] Paulo Falabella,[2,4] Roby Menefee,[5,6] John J. Whalen III,[2,3]* Mark S. Humayun,[2,3] Mark E. Thompson[1,7]

Open globe injuries are full-thickness injuries sustained to the eye wall (cornea or sclera), which cause immediate drops in intraocular pressure that may lead to retinal detachment and permanent vision loss if not treated rapidly after injury. The current standard of care for open globe injuries consists of suturing the margins closed, but the technique can be time-consuming, requires specialized training and equipment, and can lead to patient discomfort, abrasion, and infection from eye rubbing. We engineered an injectable, thermoresponsive sealant (TRS) and a custom tool to occlude open globe injuries. The smart hydrogel sealant consists of physically cross-linked *N*-isopropylacrylamide copolymerized with butylacrylate. At low temperatures, it can be injected as a liquid, and when raised to body temperature, a heat-induced gelation converts the hydrogel into a solidified occlusion. The sealant can be repositioned or removed without causing additional trauma via exposure to cold water. In vitro and ex vivo assessments of mechanical adhesion to eye tissue revealed maintenance of intraocular pressure that is five times greater than the physiological range with reversible seal strength comparable to cyanoacrylate (super glue). In vivo assessment in a rabbit model of ocular trauma demonstrated ease of use for TRS deployment, statistically significant improvement in wound sealing, and no evidence of neurotoxicity, retinal tissue degradation, or significant chronic inflammatory response after 30 days of exposure. Given the advantages of body heat–induced gelation, rapid reversible occlusion, and in vivo safety and efficacy, shape-adaptable TRSs have translational potential as smart wound sealants for temporary occlusion of surgical incisions or traumatic injuries.

INTRODUCTION

At least 2.5 million eye injuries occur in the United States each year, and open globe injuries account for 10% of these injuries (*1*, *2*). Open globe injuries can quickly escalate in complexity and yield poor visual outcomes if not managed carefully. Although incidence rates are relatively low, virtually all open globe injury patients see a reduction in visual acuity (VA), and the probability of VA loss increases with increasing time to intervention beyond 24 hours from the injury (*3*). In addition to affecting the quality of life of the patient, lifetime health care costs associated with visual impairment can approach $500,000, thus also having a major financial and societal impact (*4*).

Combat- and mass casualty–related ocular traumas are subsets of ocular injuries in which time to intervention is often delayed due to circumstances where patients are separated from medical services or triaged behind other casualties with more critical injuries. This delay in receiving treatment increases the risk for substantial visual impairment. In the U.S. campaigns in the Middle East, up to 13% of all casualties presented eye injuries, most attributed to improvised explosive devices (*5*), and between 20 and 40% of battlefield ocular injuries included penetrations to the sclera (*6*). A study of the Boston Marathon bombing determined that 13% of those injured required ophthalmology intervention (*7*). Military studies and clinical observations predict that treatments closest to the time of injury have the best outcomes (*8*). In these instances, developing a strategy to rapidly and temporarily close the globe without further trauma to the tissues is desirable.

Current treatment options for managing open globe injuries include sutures and adhesives. In general, these approaches require the use of microsurgical instrumentation accompanied by surgical microscopes to visualize tissue repair. Foreign body sensation resulting from abrasive material has been associated with eye rubbing, prolonged healing times, infection, and fibrosis (*9*). Novel bioadhesives like fibrin matrices have been used (*9*, *10*) but can carry considerable risks associated with assurance prevention of viral or prion contamination, in addition to challenges with glue deployment and ease of use. Cyanoacrylates (DERMABOND, TRUFILL, and DYMAX 222) exhibit some difficulties in dispensing and cannot be used to close globes with missing tissues (*11*). Acute inflammatory reactions in vascular tissue have been reported (*12*). There are currently no U.S. Food and Drug Administration–approved indications for using medical adhesives for closure of scleral penetrations.

Here, we propose a system designed to temporarily occlude open globe injuries. The system leverages the reversible, thermoresponsive properties of poly(*N*-isopropylacrylamide) (PNIPAM) to reversibly occlude injuries without causing additional trauma to surrounding tissues during placement or removal. PNIPAM is a smart biostable polymer investigated for a range of biomedical, drug screening, biotechnology, and medical diagnostics applications (*13*–*16*). Below about 32° to 33°C [lower critical solution temperature (LCST)], hydrophilic interactions of PNIPAM with water enable a translucent liquid state; above its LCST, it forms a partially dehydrated, soft-solid aggregate. Through copolymerization with other monomers, such as *N*-*tert*-butylacrylamide (NT) or butylacrylate (BA), we can tailor its thermoresponsive behavior and mechanical strength to create a hydrogel that shape-fills upon injection at a wound site, adapting to irregular margins and sealing traumatic injuries. The thermosensitive behavior allows the thermoresponsive sealant (TRS) to be easily removed by the application of cold water.

[1]The Mork Family Department of Chemical Engineering and Materials Science, University of Southern California, Los Angeles, CA 90089, USA. [2]USC Roski Eye Institute, Department of Ophthalmology, Keck School of Medicine, University of Southern California, Los Angeles, CA 90033, USA. [3]USC Institute for Biomedical Therapeutics, Keck School of Medicine, University of Southern California, Los Angeles, CA 90033, USA. [4]Department of Ophthalmology and Visual Sciences, Federal University of São Paulo, São Paulo 04023-062, Brazil. [5]Department of Biomedical Engineering, University of Southern California, 1042 Downey Way, Denney Research Center 140, Los Angeles, CA 90089, USA. [6]Department of Neuroscience, University of Southern California, 3641 Watt Way, HNB 120, Los Angeles, CA 90089, USA. [7]Department of Chemistry, University of Southern California, Los Angeles, CA 90089, USA.
*Corresponding author. Email: jjwhalen@med.usc.edu

We used this copolymer material to develop a reversible approach to temporarily occlude penetrating injuries to the posterior segment of the eye. In addition to tailoring the polymer chemistry, we developed a custom tool that controls the hydrogel temperature to enable effective deployment in the eye. Feasibility studies were conducted using ex vivo and in vivo models of ocular trauma in rabbits, and two user feedback workshops were held where military ophthalmologists tested the prototype systems for ease of use, general concept, and performance in an ex vivo porcine model of ruptured globe.

RESULTS

Engineered injectable TRS and mode of function

Our goal was to develop a biocompatible, tissue repair technology for temporary intervention at sites of scleral tissue damage or loss. The approach presented here involves injection of a purposefully nonbiodegradable liquid sealant capable of body heat–induced gelation to create a size-adaptable solidified occlusion, which can both restore intraocular pressure (IOP) and be easily removed within a few days for subsequent treatment without concomitant tissue damage. This technology would afford the patient a larger window of time to complete surgical intervention without requiring specialty equipment such as surgical microscopes for implementation. The system consists of two components: (i) a thermoresponsive hydrogel that, by its reversible transition from liquid to solid, conforms to wound shape and aggregates to mechanically seal scleral penetrations and (ii) a custom deployment tool to contain the hydrogel at a controlled temperature and to inject it at the targeted site (Fig. 1A).

Optimizing rheological properties of shape-persistent, moldable TRS

The physically cross-linked hydrogel with thermoresponsive behavior was designed from customized copolymer and water. The reversible transition from water-soluble coils to hydrophobic globules at the LCST changes the physical properties of the gel (Fig. 1B). Copolymerization of NIPAM with hydrophobic NT and BA not only decreases the LCST of PNIPAM but also improves the polymer's mechanical properties (*17*–*20*). By altering the compositional ratios of these copolymers, a range of formulations were synthesized via free radical polymerization and then characterized to optimize molecular weight, LCST, aqueous solution concentration, and viscoelastic properties (fig. S1). Previous studies have used both comonomers to create cell culture supports and other thermoresponsive polymers but not with synthetic uniformity or properties that met our needs (*18*, *20*). As a result, we followed a different synthetic scheme from those found in the literature and performed the necessary measurement of LCST and molecular weight for all formulations: homopolymers of NIPAM, copolymer of NIPAM with NT, and copolymer of NIPAM with BA, each using NIPAM as the main formulation component (Fig. 1C). Composition ratios for each sample were verified by ^{1}H nuclear magnetic resonance (NMR) (fig. S2).

We deliberately engineered the LCST of the polymers studied here to fall below that of PNIPAM to achieve a transition temperature for the hydrogel that is well below the eye's physiological temperature. The contributions of the NT and BA monomers to the phase transition were examined through scattering intensity measurements of aqueous PNIPAM, poly(NIPAM-*co*-NT) ($N_{85}NT_{15}$), and poly(NIPAM-*co*-BA) ($N_{95}BA_5$) solutions over temperature ranges that included their phase transition temperature (fig. S3). Higher scattering intensity was observed at higher temperatures (above phase transition temperature), which was attributed to transformation from a more soluble coil conformation below the LCST to a largely insoluble compact conformation. For instance, the scattering intensity values of $N_{95}BA_5$ exhibited sharp increases around 16°C, indicative of a gelation point. Comparison of temperature-dependent scattering intensity distributions of three different hydrogels confirmed a PNIPAM gelation point around 32°C. By inclusion of only 5% BA or 15% NT, the gelation points shifted to 16° and 22°C, respectively (Fig. 1D). We successfully engineered smart hydrogels, $N_{85}NT_{15}$ and $N_{95}BA_5$, with appropriate transition temperatures for human eye application.

The viscoelastic properties of the hydrogels were determined by rheological analysis. Conventional elastic responses at LCST were demonstrated for both $N_{95}BA_5$ and $N_{85}NT_{15}$ samples (*21*). The loss (G'') and storage (G') moduli—representations of the viscous and elastic behavior, respectively—were measured by strain amplitude sweeps across a range of temperatures (figs. S4 and S5). Without a high-enough storage modulus above LCST, the hydrogel would not be sufficiently elastic to resist intraocular pressures while maintaining an effective occlusion. Without an optimized loss modulus below LCST, the hydrogel might be too runny or thick, making it difficult to apply. The storage modulus for $N_{95}BA_5$ rapidly decreases above the critical strain region (1%), indicating gel collapse to a quasi-liquid state (Fig. 2A). For different temperatures, the respective G'' (6°, 24°, and 32°C) and G' (24° and 32°C) values of $N_{95}BA_5$ and $N_{85}NT_{15}$ were measured as a function of angular frequency at fixed strain (0.1%) (Fig. 2, B and C). We observed that hydrogel dynamic moduli depend on the temperature and that both samples reached their maximum viscosity and elasticity at 32°C. Although the mechanical strength of both hydrogels showed the same trend, $N_{95}BA_5$ generated stronger polymeric networks. Replacement of NT comonomer with BA caused the G'' and G' values to increase by a factor of up to 30.

Comparison of the viscoelastic profile of 10% (w/w) aqueous solutions of two different copolymers at eye temperature (32°C) differentiated their aggregation behavior. G' dominates over G'' for $N_{95}BA_5$, resulting in a quasi-solid state ($\tan\delta \equiv G''/G' \approx 0.4$). Under the same condition, viscosity remained relatively greater than the elasticity for $N_{85}NT_{15}$, indicating a quasi-liquid state ($\tan\delta \equiv G''/G' \approx 2.3$) (Fig. 2, D and E). $N_{95}BA_5$ was selected for further characterization, owing to its mechanical strength and desirable phase transition temperature.

Viscosity measurements of $N_{95}BA_5$ provided a better understanding of the hydrogel's conformational change (Fig. 2F). Below the gelation point, complex viscosity, η^*, was independent of temperature and constant. At and above the phase transition region, the η^* rose sharply and approached a constant value. This change resulted from copolymer dehydration, compact globule formation, and resulting polymeric networks between macromolecule chains.

The complex viscosity profiles of $N_{95}BA_5$ solutions [5, 20, and 30% (w/w)] were then evaluated to compare their concentration-dependent strength. Earlier gelation onset accompanied higher concentration, indicating that more concentrated polymer solutions form gels at respectively lower temperatures. The η^* values also confirmed that higher copolymer concentrations can improve the mechanical strength of noncovalent hydrogels. Among the three samples studied, 30% (w/w) had the greatest complex viscosity value of about 10,000 centipoise (cP) (10 Pa · s), suggesting a strong yet injectable thermoresponsive hydrogel (fig. S6). For comparison, the viscosities of honey and ketchup, two easily applied yet malleable substances, are about 3000 and 50,000 cP, respectively. The 30% (w/w) $N_{95}BA_5$ was chosen for having the most useful viscoelastic properties of the hydrogels prepared herein (Fig. 1C).

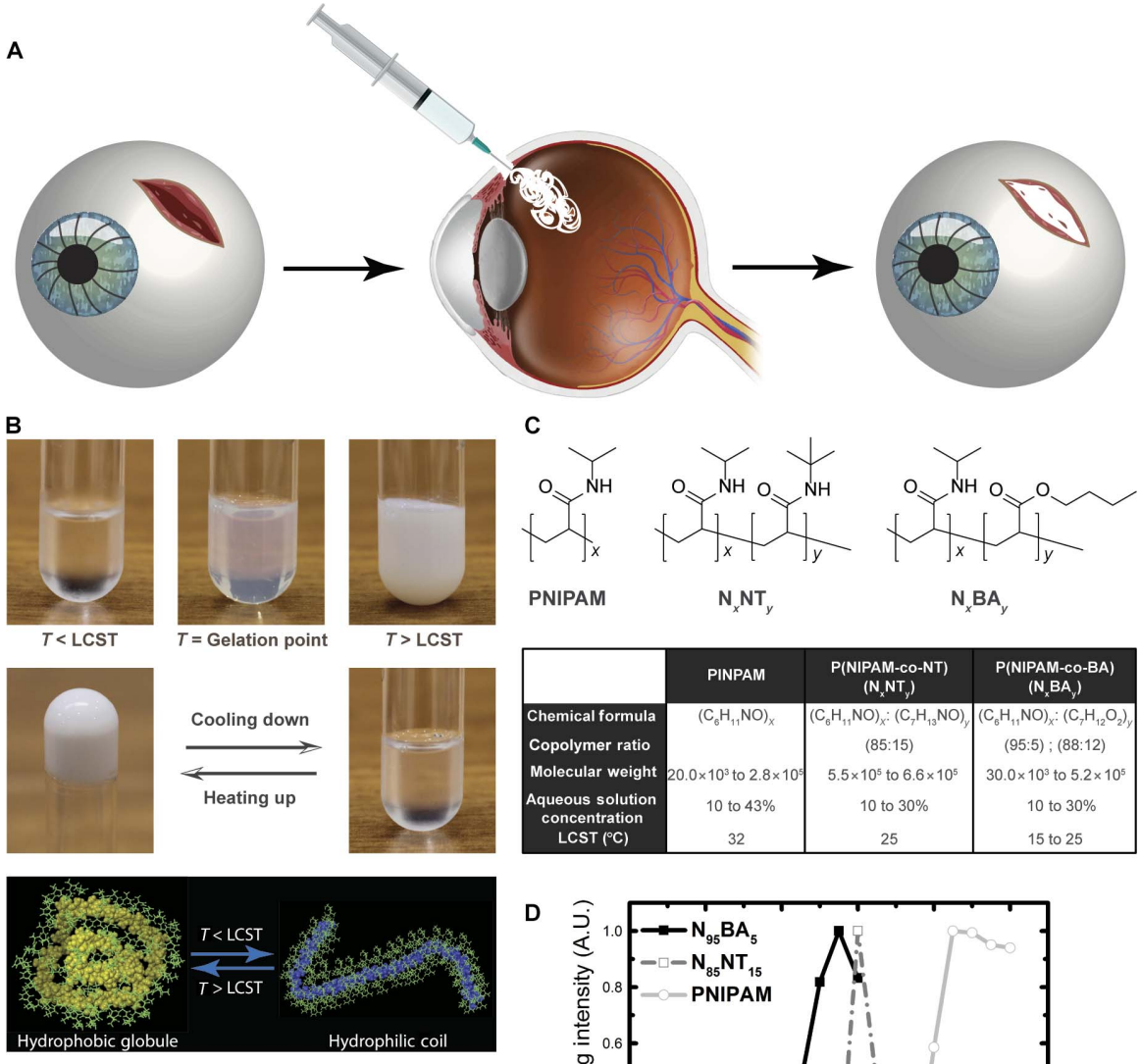

	PINPAM	P(NIPAM-co-NT) (N_xNT_y)	P(NIPAM-co-BA) (N_xBA_y)
Chemical formula	$(C_6H_{11}NO)_x$	$(C_6H_{11}NO)_x$: $(C_7H_{13}NO)_y$	$(C_6H_{11}NO)_x$: $(C_7H_{12}O_2)_y$
Copolymer ratio		(85:15)	(95:5) ; (88:12)
Molecular weight	20.0×10^3 to 2.8×10^5	5.5×10^5 to 6.6×10^5	30.0×10^3 to 5.2×10^5
Aqueous solution concentration	10 to 43%	10 to 30%	10 to 30%
LCST (°C)	32	25	15 to 25

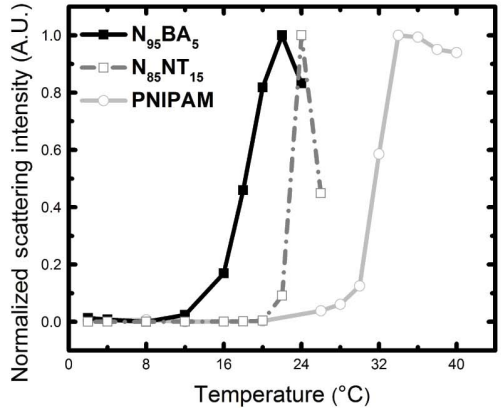

Fig. 1. Design of a thermoresponsive hydrogel to seal scleral perforation. (**A**) Schematic depicting implementation of a temperature-mediated adhesive hydrogel that adapts to wound shape and a tool for its deployment at a perforation site in the sclera. (**B**) Images of the changes in physical properties as the sealing hydrogel transitions from hydrophilic coils to hydrophobic globules at its lower critical solution temperature (LCST). (**C**) Molecular structures of formulations of poly(*N*-isopropylacrylamide) (PNIPAM) with butylacrylate (BA) or *N*-*tert*-butylacrylamide (NT) and a table of resulting alterations of molecular properties and LCST values. (**D**) Normalized scattering intensity as a function of temperature for PNIPAM, poly(NIPAM-*co*-NT) ($N_{85}NT_{15}$), and poly(NIPAM-*co*-BA) ($N_{95}BA_5$). A.U., arbitrary units.

The stiffness and resilience of the 30% (w/w) $N_{95}BA_5$ were evaluated using standard tensile and compression tests and by casting it into shapes. Compressive stress-strain curves illustrated a positive correlation between TRS concentration and compressive moduli. The results revealed that the mechanical properties of the developed hydrogel can be readily tuned by changing the hydrogel concentration, with compressive moduli modified from less than 15 to ≈55 kPa when doubling the TRS concentration from 15 to 30% (fig. S7). The elastic modulus of $N_{95}BA_5$ was characterized as a function of the concentration (20, 25, and 30%). TRS tensile stress-strain curves followed a similar trend, with increasing copolymer concentration resulting in higher Young's modulus. The 30% TRS hydrogels were found to have elastic moduli of 117 kPa, representing an improved stretching capacity compared to 60 kPa (25%) and 45 kPa (20%) (fig. S8). The resulting molded objects (Fig. 2, G to I) were resilient and sufficiently cohesive at body temperature to be suspended horizontally (Fig. 2J), vertically (Fig. 2K), and by hand (Fig. 2L). The noncovalent properties of the hydrogel also allowed it to self-heal when slightly deformed. The hydrogel satisfied critical requirements for application as an ocular sealant: moldability, persistence in form, and sufficient toughness to withstand intraocular pressure.

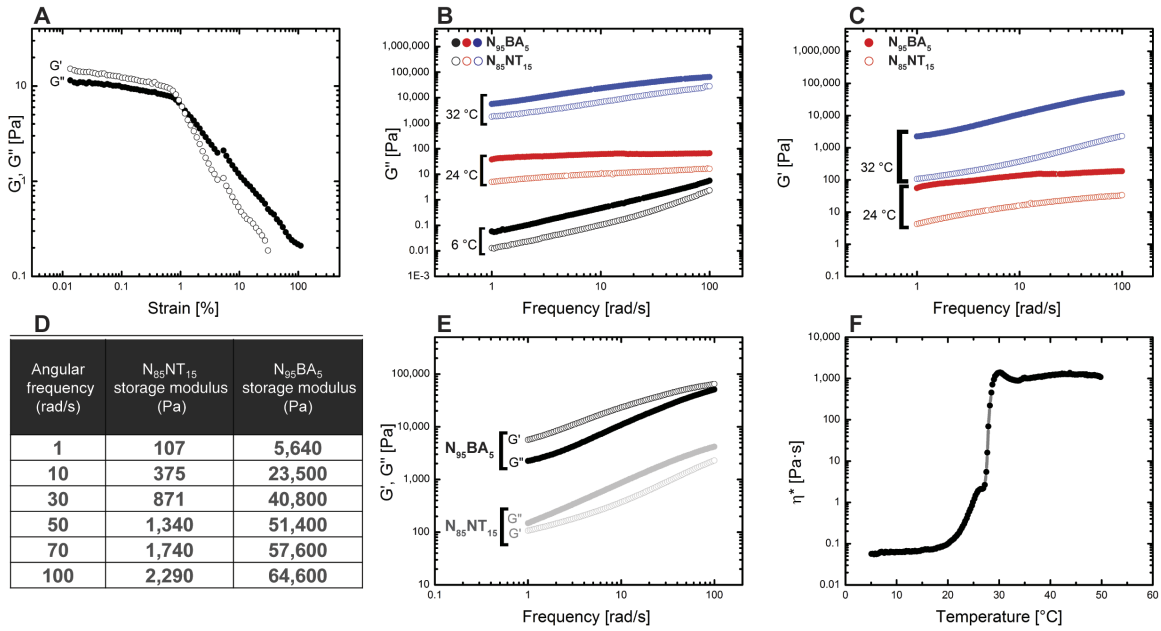

Angular frequency (rad/s)	$N_{85}NT_{15}$ storage modulus (Pa)	$N_{95}BA_5$ storage modulus (Pa)
1	107	5,640
10	375	23,500
30	871	40,800
50	1,340	51,400
70	1,740	57,600
100	2,290	64,600

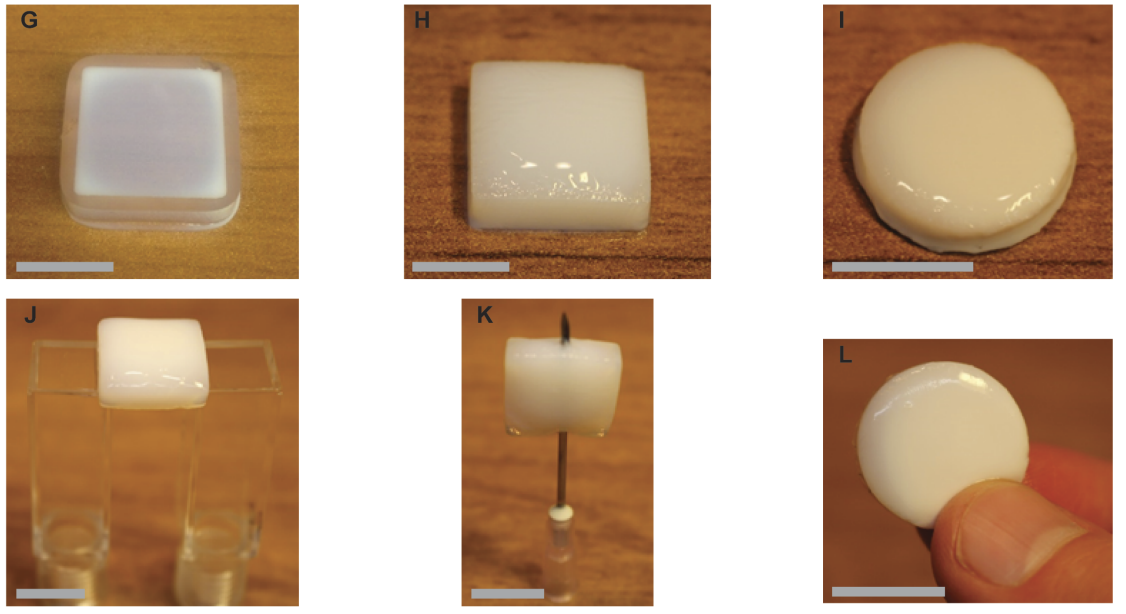

Fig. 2. Rheological characterization and hydrogel differentiation. (**A**) Storage and loss moduli (*G′* and *G″*, respectively) over strain for $N_{95}BA_5$. (**B** and **C**) *G″* (B) and *G′* (C) modulus representations of viscoelastic behavior for co-BA and co-NT as a function of angular frequency at fixed strain. (**D**) Table of storage moduli for co-NT and co-BA compositions at different angular frequencies. (**E**) Storage and loss moduli (*G′* and *G″*, respectively) over frequency for co-NT and co-BA compositions. (**F**) Measurement of complex viscosity for $N_{95}BA_5$ according to temperature. (**G** to **I**) Images of square and round gel molds formed by heating the hydrogel solutions to 32°C. Scale bars, 1 cm. (**J** to **L**) Images of solid $N_{95}BA_5$ hydrogel demonstrating horizontal resilience (J), vertical resilience (K), and strength of form on contact (L). Scale bars, 1 cm.

Ex vivo and in vitro testing of $N_{95}BA_5$ for ocular trauma

Sealant efficacy of the hydrogel was first assessed in an ex vivo cadaveric porcine eye model of ocular trauma. Cyanoacrylate was selected over fibrin-, albumin-, and polyethylene glycol–based adhesives as a positive control because of its well-documented superiority in maintaining IOP and uniaxial adhesion strength (*22*, *23*). The hydrogel was applied to the lacerated eye model after an incision procedure (Fig. 3A). The hydrogel was injected into the posterior chamber of the eye through the perforation, and the injection tool was slowly retracted while continuously deploying the hydrogel, leaving a sealant trail through the wound. At the exterior surface of the sclera, additional hydrogel was deposited, creating a gel rivet-like cap. The caps were left to settle for several seconds, allowing them to increase in temperature and dehydrate before being cut away or smoothed flat (Fig. 3, B and C). IOP was then controllably raised by infusion with warm saline from the cannula inserted in the posterior chamber.

By comparing the IOP values established at eye temperature (32°C) by 15, 20, and 30% (w/w) aqueous solutions of $N_{95}BA_5$ and $N_{85}NT_{15}$, $N_{95}BA_5$ was determined to be the superior hydrogel, maintaining ocular pressures above 70 mmHg for all concentrations. Under the same conditions, IOP values for 15 and 20% $N_{85}NT_{15}$ were less effective,

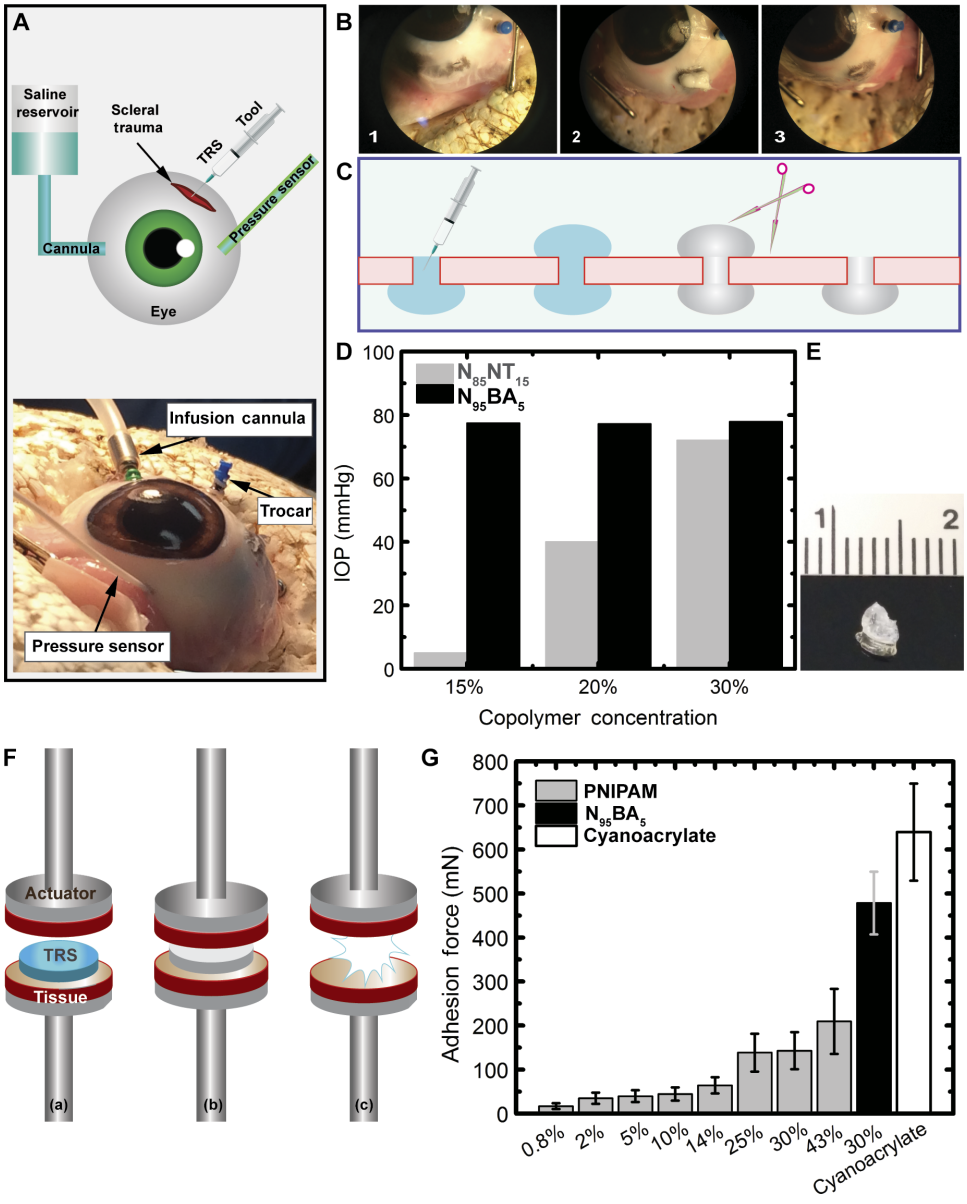

Fig. 3. Preliminary ex vivo and in vitro hydrogel evaluation. (**A**) Schematic (top) and image (bottom) depicting ex vivo procedures carried out in a pressure-controlled explanted cadaveric pig eye. (**B** and **C**) Images (B) and schematic depiction (C) of hydrogel injection through scleral perforation by deployment of a sealant trail through the wound, leaving rivet-like caps subsequently removed to leave the occlusion flush with the scleral surface. (**D**) Comparison of maintained intraocular pressures across a concentration spectrum for $N_{95}BA_5$ and $N_{85}NT_{15}$ hydrogels (n = 3 per group). (**E**) Image of a solid plug removed from a test eye. (**F**) Schematic depicting tissue adhesion tests comparing PNIPAM, $N_{95}BA_5$, and cyanoacrylate adhesion strength to scleral tissue ex vivo. (**G**) Adhesion force of different concentrations of $N_{95}BA_5$, PNIPAM, and cyanoacrylate to scleral tissue; columns show 478 ± 71 and 639 ± 110 for $N_{95}BA_5$ and cyanoacrylate, respectively (n = 3 per group).

containing pressures of 5 and 40 mmHg, respectively (Fig. 3D). Although high concentrations (30%) of both $N_{95}BA_5$ and $N_{85}NT_{15}$ hydrogels were capable of maintaining pressures of up to 72 mmHg, leakage was observed for $N_{85}NT_{15}$, indicating a quasi-sealed state. Even so, the formulations identified as effective could withstand IOPs of up to 77 mmHg without leakage, an environment approximately five times the physiological IOP range. Both the $N_{95}BA_5$ samples and a cyanoacrylate-sealed positive control held the maximum pressure (78 mmHg) of our experimental setup, demonstrating effective equivalence. In contrast, our negative control without a sealant held no pressure. Figure 3E shows a hydrogel plug removed from one of the rabbits at the end of the study.

Although we designed the hydrogel as an ideal mechanical sealant, in vitro uniaxial adhesion tests were performed to provide accurate comparison between the adhesion force of cyanoacrylate, the strongest ocular adhesive, and our TRS. The hydrogel or cyanoacrylate was sandwiched between two pieces of dissected scleral tissue that were fixated to the base and actuator arm of a pull tester (Fig. 3F). Apposed tissues were brought down and pressed together using 15g of pressure for 2 min. The actuator was then pulled until the two tissue samples detached. In addition to the 30% $N_{95}BA_5$, different aqueous concentrations of PNIPAM ranging from 0.8 to 43% (w/w) were chosen to assess the impact of concentration. Adhesion results of homopolymers suggested that an increase in the aqueous concentration of the hydrogel increased the adhesive strength between the hydrogel and scleral tissue. Adhesion forces between 336 and 560 mN were observed for the 30% (w/w) $N_{95}BA_5$ before adhesion failure at the tissue-hydrogel interface. Under the same uniaxial conditions, cyanoacrylate's adhesion force was slightly higher (Fig. 3G). Wetting, diffusion, and adsorption theories offer mechanical and molecular explanations for this behavior but were not explored in this study (*24*, *25*).

In situ gelation mechanism of TRS in the eye

Ex vivo application indicated that to occlude the incision properly, the hydrogel must change from transparent liquid to white solid (Fig. 3B). We used dynamic light scattering (DLS) techniques to obtain particle size in solution, gel and solution-to-gel transition states, and particle impact on gelation kinetic and mechanical properties. At 2°C, below LCST, we observed that 96% of the intensity corresponds to particles with a small hydrodynamic radius (3.6 nm), attributed to single polymer chains in the coil conformation (Fig. 4A). At the phase transition region, we observed two peaks with comparable intensities. One peak (236.2 nm) corresponded to $N_{95}BA_5$ molecules that were partially aggregated in the solution, and the other peak (4.5 nm) corresponded to lower-radius particles (Fig. 4B). Further temperature increase to 20°C caused 98% of the copolymer to form large aggregates (439 nm), a consequence of more favorable polymer-polymer

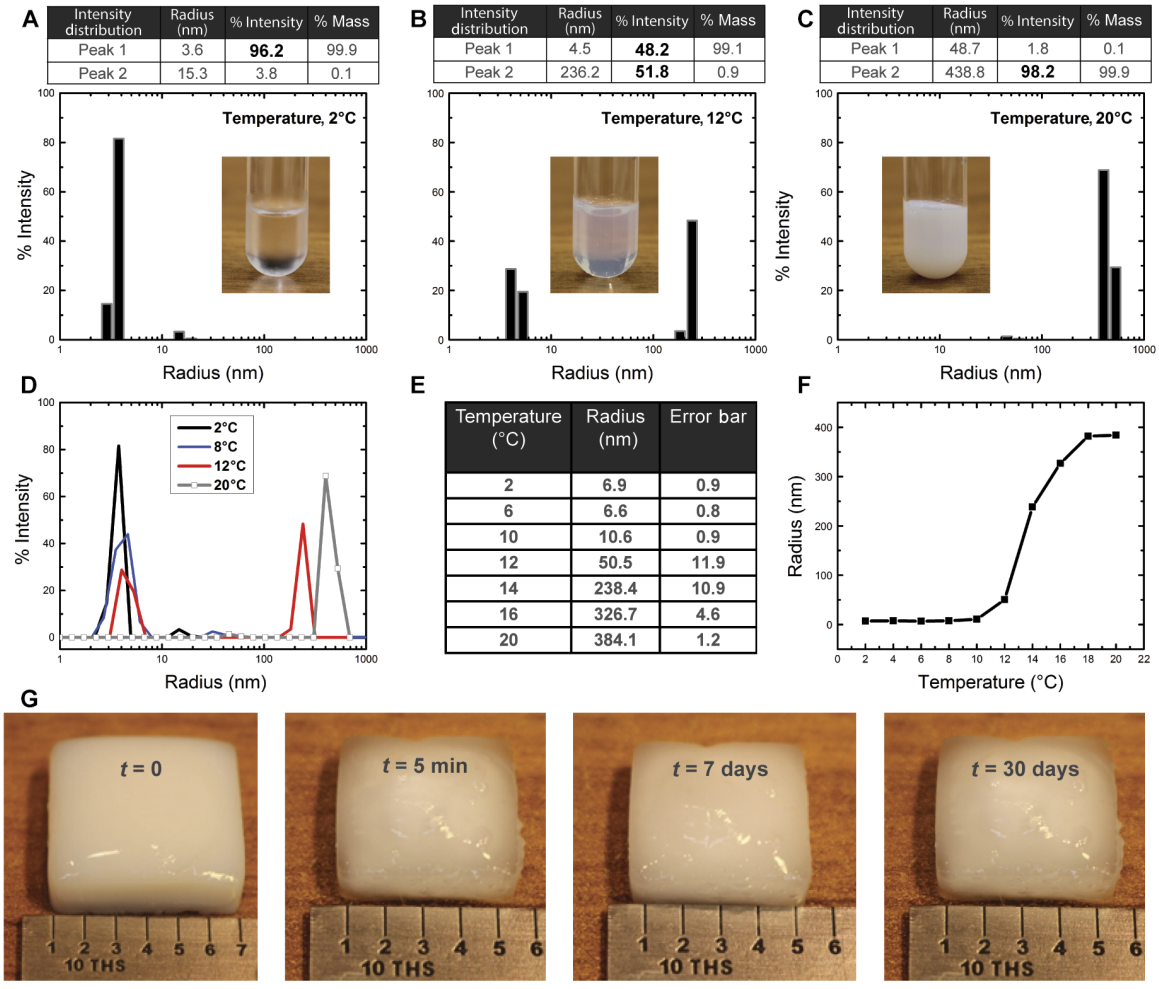

Fig. 4. Hydrogel particle size and gelation mechanism. (**A**) $N_{95}BA_5$ particle size as assessed using dynamic light scattering in solution below LCST (2°C), showing a 96% scattering intensity for small-radius particles. (**B**) Particle size in the phase transition region (12°C). A split was observed between particles with hydrodynamic radius of 4.5 and 236.2 nm. (**C**) Particle size toward the end of the phase transition region (18°C). Ninety-eight percent of scattering intensity was due to large-radius $N_{95}BA_5$ aggregates. (**D** to **F**) Hydrodynamic radius size of particles traced through the hydrogel transition to show higher aggregate populations at higher temperatures (n = 3 per temperature). (**G**) Gross images of molded hydrogel samples held at the expected eye temperature (32°C) for up to 30 days, showing slight volume decrease and good shape persistence and stability.

interactions (Fig. 4C). Amide groups facilitated those interactions by forming hydrogen bonds between polymer molecules, nesting themselves inside the globules.

Intensity distribution across a range of temperatures (2° to 20°C) allowed further characterization of the temperature-induced hydrophobic aggregation process (fig. S9). For brevity, the size distribution graphs of only four temperatures (2°, 8°, 12°, and 20°C) were included (Fig. 4D). With temperature increase, the first peak corresponding to smaller particles decreased in size. Simultaneously, hydrodynamic radius (R_H) and intensity of the high aggregation peak region increased with heat (Fig. 4D).

Analysis of R_H values for $N_{95}BA_5$ aggregates provided detailed understanding of the gel's temperature dependence. At temperatures below the LCST, R_H remained nearly constant (<10 nm) up to 10°C, but increasing the temperature above the 12°C gelation onset condition led to a rapid increase in the hydrodynamic radius and to sizes markedly larger than the PNIPAM aggregates (*26*). Greater aggregate size makes for better ocular sealant because larger particles diffuse less readily into the vitreous gel, as predicted by the Stokes-Einstein equation. The aggregation onset temperature was confirmed by the results of scattering intensity tests. DLS measurements could not be performed above 20°C because of the turbidity gain of the hydrogel solution (Fig. 4,E and F). In summary, the nanometric copolymer aggregates associate upon exposure to heat, becoming insoluble in aqueous solution as a consequence of more favorable polymer-polymer interactions.

As observed previously, heated hydrogel can form shape-persistent objects by in situ gelation. The thermo-induced volume change of these molded shapes was further characterized to investigate hydrogel stability in an environment similar to the eye. The swollen hydrogel underwent slight volume reduction after only 5 min of exposure to 32°C deionized water. Shape persistence and stability remained for 1 month in an aqueous environment above its LCST (Fig. 4G). These formed shapes were also maintained at 10°C, below LCST, resulting in complete structural collapse after a few hours, consistent with the thermoresponsive trends observed (fig. S10). Our hydrogel challenges the preconception that materials held together by noncovalent forces and mostly composed of water are weak.

Effective TRS deployment in an in vivo model of ocular trauma

Effective deployment of the hydrogel without premature transition required development of a controlled-environment injector tool to meet optimal use requirements derived from clinical end users (table S1). The preliminary design consisted of a 1-cm^3 chamber inside a larger 15-cm^3 thermal jacket (Fig. 5A, a) in an easily used form factor. On the basis of the preliminary design and volume of space available inside the thermal jacket, a series of endothermic chemical reactions of ammonium nitrate salt and water was performed and optimized to rapidly cool the hydrogel chamber to 0°C within 60 s of mixing and to maintain the hydrogel's temperature between 0° and 10°C for up to 10 min (Fig. 5A, b). A working prototype was fabricated from off-the-shelf parts, including a 1-cm^3 syringe nested inside a larger 15-cm^3 syringe and a soft removable loading port cap, which allowed ammonium nitrate to be loaded into the jacket and water to be injected in the jacket when ready for

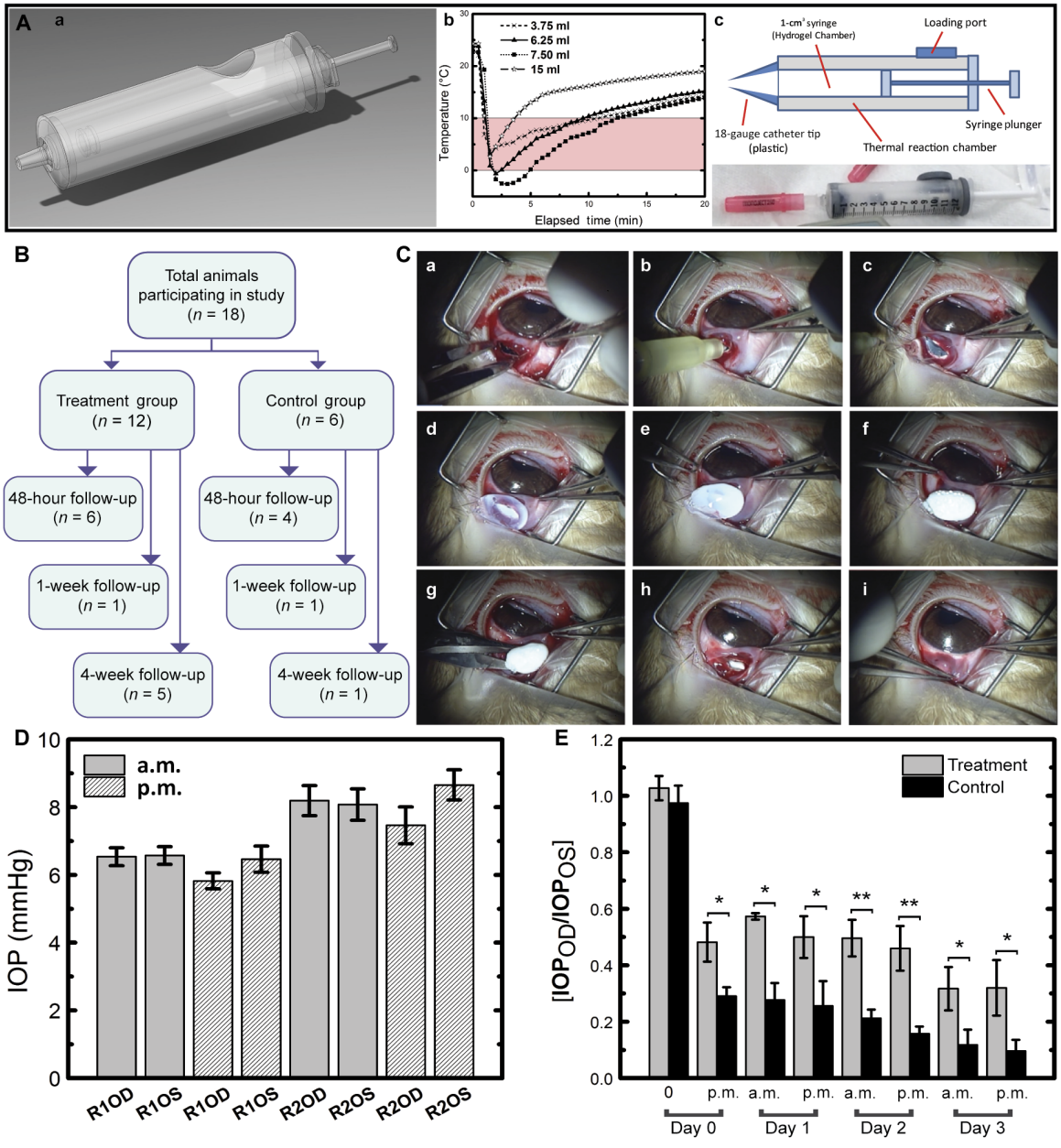

Fig. 5. Preliminary performance validation of the hydrogel in vivo in a rabbit model of scleral trauma. (**A**) Design diagrams (a and c) and validation (b) of a custom injection tool to effectively control hydrogel deployment and regulate its temperature. An image of the prototype injector is shown in the bottom right. (**B**) Two-arm study design to assess safety and efficacy of the hydrogel versus the current standard of care for posterior segment open globe injuries. (**C**) Images of the surgical procedure in rabbits. A 3-mm, full-thickness linear incision was created in the sclera about 3 mm radial from the limbus, followed by preparation and deployment of the hydrogel through the incision. (**D**) Representative baseline intraocular pressure (IOP) values showing no statistical difference between eyes of the same animal or any circadian-induced variations; columns show 6.5 ± 0.2, 6.5 ± 0.2, 5.8 ± 0.2, 6.4 ± 0.3, 8.1 ± 0.4, 8.0 ± 0.4, 7.4 ± 0.5, and 8.6 ± 0.4 mmHg (n = 28 per group). (**E**) Wald test comparison of mean IOP values of the treatment group versus no intervention, after procedure, showed a statistically significant improvement in mean IOP with sealant placed (*P < 0.05 and **P < 0.001).

use (Fig. 5A, c). Cooling characteristics were optimized by varying reactant concentrations and tracking temperature transients to achieve the desired deployment window (fig. S11). A polymer-based catheter cannula was also used on the injector tip for hydrogel application to reduce thermal conductivity from the eye, which could have induced temperature transition solidification in the tool's lumen during deployment.

An in vivo pilot validation study was performed in a rabbit model of ocular trauma to assess the ease of use, safety profile, and preliminary efficacy of the $N_{95}BA_5$ hydrogel. A 7-day in vivo follow-up study was performed to compare the performance of the hydrogel wound closure versus no intervention (control). A subset of the study animals were followed for an additional 3 weeks (4-week endpoint) to more carefully examine safety and potential inflammatory responses to hydrogel placement in the eye (Fig. 5B and table S2).

For each test run, a 3-mm full-thickness laceration was created in the sclera to simulate a penetrating injury (Fig. 5C, a). After trauma creation in a treatment group rabbit, the tool was inserted into the laceration (Fig. 5C, b) and the hydrogel was deployed (Fig. 5C, c). Once deployed, the hydrogel was then allowed to set for 5 min, enabling the dehydration transition from translucent (Fig. 5C, c and d) to an opaque white color (Fig. 5C, e). Expelled water formed visible droplets on the gel surface (Fig. 5C, f). The rivet cap formed on the ocular surface was then cut away to create a low-profile, flat head (Fig. 5C, g to i). The procedure can be viewed in movie S1. Ease of use of deployment was evaluated by comparing the number of successful hydrogel placements into the eye versus the number of hydrogel placement attempts.

Despite limited training with the system, the veterinary surgeon was able to successfully deploy the hydrogel on the first attempt in greater than 80% of the cases (table S2). During follow-up, trauma sites in the control group were difficult to locate. The conjunctival epithelium formed a fibrotic layer across the margins in an attempt to repair the breach. Although suggestive of a natural healing process, the eyes still exhibited hypotony with IOPs of ≤4 mmHg, likely attributable to a leaky, porous closure.

The scleral surface of all study eyes [right eye (OD)] was visually evaluated by an ophthalmologist at 24 hours, 48 hours, and 1 week to look for signs of scleritis or other vasculitis of surrounding tissues that might be indicative of adverse tissue responses to the hydrogel material (fig. S12). Despite some signs of acute inflammation in the first hours (less than 12 hours) after the original procedure, irritation rapidly subsided. By the 24-hour mark, treatment and control eyes were barely distinguishable. Evaluation at 48 hours after surgery revealed no hyperemia or inflammation at the treatment site, which persisted until study termination.

Hydrogel efficacy in situ was evidenced by IOP restoration to normal ranges and negative Seidel test, the standard clinical test for identifying ocular leakage/dehiscence. Mean baseline IOP values showed no statistically significant difference between the study eye (OD) and fellow eye (OS) of each animal (presurgical OD/OS between groups, $P = 0.35$), consistent with previous reports (Fig. 5D) (*27*). Immediately after incision creation, both treatment and control groups showed significant decreases (>80%) in mean-normalized IOP. As restoration of IOP relied on physiological production of aqueous humor, immediate improvement in IOP was not expected in both groups.

A noticeable IOP increase occurred about 12 to 24 hours after procedure in the treatment group, and statistically significant improvement in IOP continued over the 72 hours after placement of the hydrogel relative to the control (Fig. 5E and table S3). Normalized mean IOP measurements across all time points beyond 24 hours after procedure showed statistically significant improvement over control, with an even greater improvement noted beyond 48 hours ($P < 0.05$). Normalized to the mean normal clinical IOP (15.5 mmHg), the lower threshold for normal human IOP pressure (10 mmHg) becomes 65% (*28*), and unrepaired globes maintained a low IOP no greater than 30% of normal. In stark contrast, hydrogel closure consequently raised IOP to 90% of the minimum threshold for normal IOP and sustained IOPs almost twice the magnitude of no treatment.

$N_{95}BA_5$ biocompatibility up to 1 month after ocular implantation

Histological analysis was performed at 48 hours, 1 week, and 4 weeks after hydrogel implantation to investigate potential adverse reactions. Tissue cross sections with the laceration and hydrogel placement sites marked (Fig. 6A, black arrows) show the trauma site and hydrogel placement location. A comprehensive analysis of tissue reaction over intervention time course was drafted by a certified pathologist (table S4). Despite design intent for acute intervention, elongated exposure allowed inspection of chronic inflammatory reactions, usually observed at 3 to 4 weeks after an implantation (*29*).

At 48 hours, control group wound margins appeared clean with the presence of some acute inflammatory cells (Fig. 6A, top left). Partial evulsion of peripheral retina was noted at the margins (blue arrow) of the control group along with some inward epithelial migration (red arrow). At 1 week, the control eyes exhibited a typical acute inflammatory response, forming a porous fibrotic layer bridging the lesion margins that matured from a positive Seidel test (confirmed leakage) to a complete IOP-supportive barrier by week 4. At week 1, there was no evidence of inflammation or infection in scleral tissues, but epithelial migration into the posterior chamber was observed. Trichrome staining revealed the mature (week 4) barrier to be dense and primarily composed of collagen fibers, a natural healing response. Small distributions of inflammatory markers were found in the newly formed tissues, but there was no evidence of chronic inflammation.

Treatment group eyes exhibited similar clean laceration margins at 48 hours with some retinal tissue evulsion; however, the opposing margins were noticeably separated (Fig. 6A, right) as a result of the hydrogel occlusion. Acute inflammatory cells at wound margins and slight inward epithelial layer migration were consistent with acute traumatic injury. An immature encapsulation layer formed over the wound by week 1, with no evidence of lesion closure or epithelial bridging, providing a quantitative metric for the foreign body reaction (Fig. 6B). The layer had a moderate thickness (51.0 ± 15.7 μm) of 10 to 20 cell layers. At 4 weeks, the encapsulation matured into a compact (13.4 ± 4.9 μm) tissue layer lining the margins of the lesion. Trichrome staining confirmed this layer to be rich in collagen, indicating evidence of a mature and compact fistula with a minimally adverse tissue response and no evidence of chronic inflammation forming around the hydrogel plug. The sclera also created an immature encapsulation layer containing some inflammatory cells, which separated the scleral tissue from the implant. Despite small quantities of infiltrate observed in the scleral margins at week 1, there was no evidence of sustained or excessive infiltrate, giant cell formation, or other chronic inflammation indicators at week 4.

Treatment group retinas showed no evidence of detachment and showed no evidence of neurotoxicity after 4 weeks of exposure (Fig. 6C). Different approaches have been used previously to assess neurotoxicity, including neurophysiological electroretinogram recordings

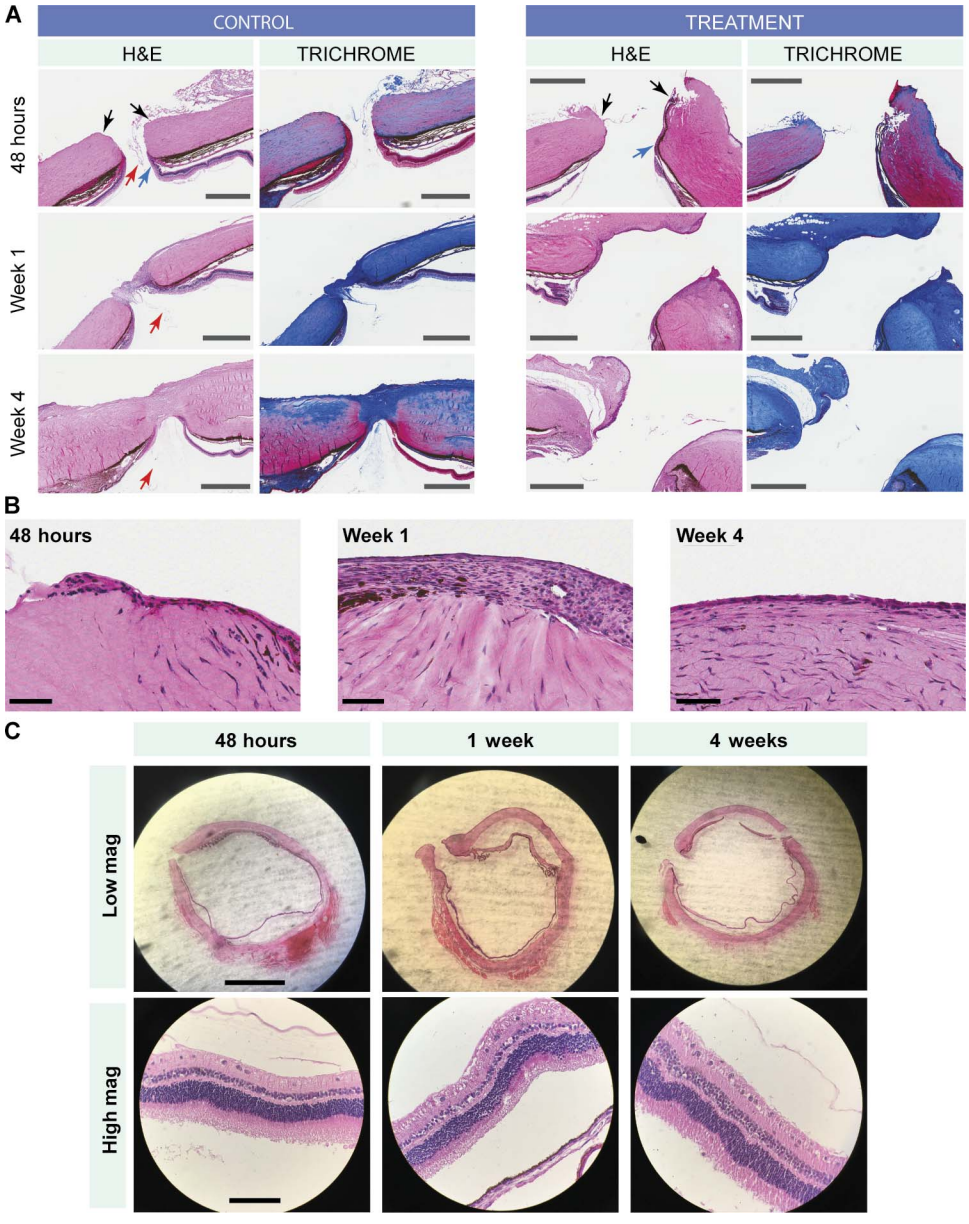

Fig. 6. $N_{95}BA_5$ biocompatibility beyond intended use frame. (**A**) Series of histological cross sections prepared for control (left pairs) and treatment (right pairs) in hematoxylin and eosin (H&E) and Masson's trichrome stain for each of the study endpoints (t = 48 hours, 1 week, and 4 week). Scale bars, 800 μm. (**B**) Increased magnification of one of the laceration margins for the treatment group showing evolution of the tissue-hydrogel interface from acute inflammatory infiltrate to a mature, compact fibrotic encapsulation layer at 4 weeks. Scale bars, 50 μm. (**C**) Gross visualization (top row) and high-magnification (bottom row) evaluation of treatment group retinas showing no evidence of trauma-induced retinal detachment or hydrogel-induced retinal neurotoxicity. Scale bars, 5 mm (top row) and 100 μm (bottom row).

and histological study of retinal structure (*30*). Treatment group physical retinal evaluation showed no signs of photoreceptor outer segment degeneration or other evidence of disorganization in the laminar tissue structure (Fig. 6C, bottom row). Organized ganglion cell layers, inner and outer plexiform layers, and nuclear layers were also present, along with retinal photoreceptor outer segments, all consistent with normally functioning retina. Any separation between the retina and choroidal layers was confirmed as artifacts of the histological slide preparation, which is a common observation (*31*). Even 30 days after implantation, the treatment group retinal tissues showed no signs of degradation or detachment.

User feedback workshop with military ophthalmologists and technicians

To validate the potential implementation of this technology in the clinic, two user feedback workshops were organized to allow military clinical personnel, who might see ocular trauma casualties, to use the TRS system in a benchtop model of ruptured globe injury (fig. S13). Two user feedback workshops that collectively captured end user feedback from 53 clinicians (ophthalmologists, physicians, medics/technicians, and researchers) with experience or career interests in managing ocular trauma in combat casualties were organized. The objective of these exercises was to assess the clinical relevance of the technology design and to capture any additional design refinements.

Each participant was given a brief tutorial and then asked to treat an enucleated pig eye with a full-thickness scleral laceration (0.5 to 2.0 cm in length). Each participant was given two attempts to close the globe. After sealant placement, warm saline was infused into the eye via a cannula to test integrity. Forty-three percent of the participants were able to successfully deploy the hydrogel at the site to effectively occlude the ruptured globe on the first attempt. All of the participants (100%) were able to successfully deploy the hydrogel at the site of the injury and close the globe in two attempts.

A questionnaire was administered to the participants with write-in (table S5) and multiple choice (table S6) questions. Of the responses collected, 69% of the respondents (n = 22) thought the idea of the reversible occlusion for open globes was a good idea (table S5), with 59% thinking it was great. Thirty-one percent found the system easy to use, with 25% noting that the system required minimal training. Perhaps most interesting, 94% of the responders (n = 30) said that they could envision the system being used in the field or in managing combat casualties.

DISCUSSION

PNIPAM and its copolymers have been extensively explored, but the combination of NIPAM and BA to target a biologically relevant transition temperature and mechanical properties pursues a unique trajectory.

Previous studies have imbued custom copolymers with the temperature sensitivity of PNIPAM, achieving pH-resistant graft copolymers, altered LCSTs, and temperature-dependent drug diffusion (*13*, *32*). Responsive properties of PNIPAM have also been applied to acylated polymer-bound parylene C for temperature-mediated tissue binding (*33*). With these dynamic modifications in mind, PNIPAM was an obvious foundation for an impermanent, biological sealant. To be used in the eye at 32°C, however, the LCST needed to be lowered.

Selection of the ideal copolymer conformation required examination of temperature-dependent aggregation behavior. Previous studies of PNIPAM copolymer behavior have used viscosity and DLS measurements to characterize particle size and shape (*34*). Our findings verified the concentration-dependent properties of hydrogel aggregation for this engineered conformation—higher concentration slightly lowered LCST—and reaffirmed non-Newtonian characteristics observed in studies of additive effects (*35*, *36*). The quasi-solid state of the 30% $N_{95}BA_5$ hydrogel, in conjunction with its lowered LCST, distinguished it as the ideal candidate. Potential further improvements to the aggregation process could be explored via the heating protocol as a sample's temperature history can affect rheological properties (*37*).

Successful completion of the hydrogel design and characterization enabled advancement to preliminary ex vivo and in vitro performance and safety assessments. Hydrogel plugs maintained IOPs greater than normal physiological IOP, suggesting the possibility of prolonging the injury-to-operation window, but doing so with a reversible sealant. In addition, the non-Newtonian state of $N_{95}BA_5$ allowed it to adapt to wound irregularities and also exhibit self-healing characteristics. This resilience has been noted in other noncovalent hydrogels, supporting the idea that these moldable materials can exhibit significant mechanical strength (*21*). In contrast, the NT comonomer proved less effective at maintaining high IOPs in the ex vivo test protocol, a result that paralleled reports of *n*-butyl cyanoacrylate scleral sealants preventing high IOP leaks in similar models (*38*).

The in vivo study provided preliminary insight into the hydrogel's efficacy in occluding open globe injuries. Whereas control groups approached 30% of normal pressure, treatment group IOP reached as high as 60%, which was corroborated by negative Seidel tests. The hydrogel formed a barrier capable of improving IOP during a 72-hour wait time for treatment.

Our preliminary biocompatibility assessment of $N_{95}BA_5$ suggests no significant adverse effects. Most reported studies on PNIPAM biocompatibility for biomedical and cosmetic applications support our findings (*39*–*42*); however, there has been one report of some observed tissue inflammation (*43*) and another reporting IOP decrease (*44*). No such history of testing exists for the hydrogel studied here, but PINIPAM copolymerized with BA has demonstrated basic cell compatibility (*45*). Our examinations demonstrated no neurotoxicity, no retinal tissue degradation, and no significant chronic inflammatory response after sustained exposure (30 days). Study limitations have now been addressed in this paragraph, and after an exhaustive literature review, we are not aware of any further material limitations. This preliminary demonstration of safety still requires a larger study size to rule out effects on retinal function.

Clinical user feedback is a valuable element in developing new interventions and therapies, and here, we specifically targeted military clinicians, who have encountered or who will encounter ocular trauma under conditions where temporary intervention may be preferable over full intervention. Although full intervention at first admission is preferred (*8*), some scenarios, such as mass casualty events, may create scenarios where multiple ocular injuries may delay intervention (*7*). The feedback captured from the military clinicians provided some good validation that the ease of use and the relevance of the technology were both real.

This study establishes foundational feasibility, safety, and efficacy of $N_{95}BA_5$ as a reversible thermoresponsive hydrogel for temporary closure of scleral perforations. This tissue repair technology sustained IOPs five times greater than the physiological range in bench testing of maximum adhesion, prevented hypotony for 72 hours after scleral trauma, and demonstrated sufficient biocompatibility for exposures longer than the intended use period. Furthermore, the hydrogel's adaptability to wound shape and unique deployment method make a unique and easy alternative to conventional methods.

MATERIALS AND METHODS

Study design

The overall objective of this study was to assess the feasibility of developing a temporary ocular repair technology with physical and mechanical properties suited to improving outcomes for globes compromised by scleral tears. This objective was segmented into three efforts: a polymer chemistry investigation of hydrogel properties correlated to synthesis route and composition, a materials science study of performance characteristics using benchtop models of ocular trauma, and an in vivo, preclinical study of safety and performance in an animal model of ocular trauma. Our initial work evaluated the potential of two compositions at different concentrations. These copolymers incorporated hydrophobic monomers (NT and BA) with NIPAM to form a temperature-responsive hydrogel in water with improved mechanical strength. Preliminary evaluation consisted of transition temperature's shift verification by scattering intensity, followed by examination of storage and loss moduli for relative viscoelastic properties. Identification of $N_{95}BA_5$ as the preferred sealant was followed by compression, tension analysis, and tissue adhesion tests at eye temperature. Secondary evaluation consisted of in vitro and ex vivo testing of different concentrations of the $N_{95}BA_5$ hydrogel in appropriate porcine test models. These tests led to further narrowing of the potential candidate compositions to only the 30% (w/w) $N_{95}BA_5$ for advancement to in vivo performance and safety testing.

The sealant technology safety and performance were assessed in an in vivo model of ocular trauma. A 2:1 (treatment/control) randomized and unblinded study was designed to evaluate the hydrogel sealant against the envisioned standard of care (no intervention). All animals (n = 18) received a 3-mm full-thickness laceration through the sclera, and treatment arm animals (n = 12) received the hydrogel sealant. All animals had regular IOP measures taken in triplicate at each time point to calculate a mean IOP for each time point. Animals were followed to one of three study endpoints (48 hours, 1 week, and 4 weeks), after which eyes were enucleated and fixed for histological preparation and analysis. Tissue segments were examined for evidence of adverse tissue responses including chronic inflammation, retinal degradation, cytotoxicity, and neurotoxicity.

Homopolymer and copolymer synthesis

PNIPAM, copolymer of NIPAM and NT ($N_{85}NT_{15}$), and copolymer of NIPAM and BA ($N_{95}BA_5$) were synthesized using free radical polymerization (*44*, *45*). For $N_{85}NT_{15}$, a solution of NIPAM (4.25 g), NT (0.75 g), and 2,2′-azobisisobutyronitrile (0.021 g) was dissolved in 60 ml of dry tetrahydrofuran (THF). The magnetically stirred solution was degassed, heated to 50°C for 24 hours under positive nitrogen pressure, and

allowed to cool. The reaction mixture was filtered (0.45-μm Teflon filter), and the filtrated volume was reduced by half. Ether was added with mixing to precipitate the copolymer. The precipitate was filtered off, washed with ether, and dried under vacuum to yield dry 4.64 g of copolymer product. For $N_{95}BA_5$, we followed the same procedure except that we used a different ratio of NIPAM (4.75 g) to BA (0.25 g). Using different ratios of THF/benzene as a solvent, we were able to synthesize homopolymers and copolymers with various molecular weights and polydispersities. After differentiation of the hydrogel compositions and the identification of $N_{95}BA_5$ for further application, the copolymer was then purchased from Sigma-Aldrich.

^{1}H NMR

Feed ratio accuracy was confirmed by ^{1}H NMR (Varian VNMRS-600). We prepared 5% (w/w) solutions of $N_{85}NT_{15}$ and $N_{95}BA_5$ in $CDCL_3$. Peak integration ratios were compared to theoretical ratios for compositional verification.

Hydrogel solution preparation

The required amount of PNIPAM, $N_{85}NT_{15}$, and $N_{95}BA_5$ was weighed for various concentrations of hydrogel aqueous solutions, from 0.8 to 43.2% (w/w). The powder was added directly to the sterile water. The vial containing the polymer suspension was then processed with a Misonix Sonicator 3000 using a cup horn high-intensity ultrasonic water bath at the maximum power setting (10) due to sample viscosity. A circulating temperature control water bath held at 2°C prevented sample heating due to prolonged horn activity. The sample was sonicated until a transparent clear hydrogel was obtained. The required sonication time ranged from 1 to 30 hours and depended on the hydrogel concentration and molecular weight of the homopolymers/copolymers.

Scattering intensity analysis

Scattering intensity measurements of 5% (w/w) hydrogels were carried out using a Photon Technology International Quantamaster fluorescence spectrophotometer. All intensity measurements were performed at an excitation wavelength (λ_{ex}) of 450 nm, with detectors positioned 90° from the light source. Emission spectra were recorded with a slit width of 0.1/0.1 nm. Quartz cuvettes (1 cm × 1 cm × 3 cm) containing the sample were placed in a cell holder, which was electrothermally controlled at a precise temperature regulated by a Peltier cooler. Each hydrogel was left under undisturbed conditions for 20 min at each temperature to obtain thermodynamic equilibrium.

Because the input light source was directed at the sample, the particles redirect the light away from a direct course through the cuvette with increasing severity as particle size increases. For small particle sizes, most of the input beam traverses the sample directly, resulting in small scattering measurements. As particle size increases, more of the light affects the particles, resulting in sideways diffusion of light that could be focused and then received by the sensor at 90° to the input beam. Scattering values were then normalized. Because of increase in sample opacity above LCST, most of the input beam was eventually reflected upon initial contact with the sample. As a result, higher temperatures saw a slow decrease in intensity because less input beam reached the center of the sample to be scattered toward the receiver.

Rheological analysis

An Anton Paar Modular Compact Rheometer (MCR) was used to measure the rheological properties of hydrogels. Eight milliliters of 10% (w/w) $N_{95}BA_5$ and $N_{85}NT_{15}$ hydrogel solutions was placed into the cylinder with special care to avoid evaporation of water. First, the hydrogels were investigated with strain-amplitude sweeps below their LCST (6°C), at LCST, and above the transition temperature (32°C) at constant angular frequency (10 rad s^{-1}). After the critical strain was found for each hydrogel, oscillation tests were performed to measure the loss (G'') and storage (G') moduli at a designated temperature (6°, 24°, and 32°C) using a circulating temperature control water bath. Strain was fixed at 0.1% (below the critical strain), and moduli were measured as a response to logarithmic angular frequency ramp from 0.1 to 1000 rad s^{-1}. Temperature-dependent changes in complex viscosity were performed using a fixed angular frequency of 10 rad s^{-1}, 0.1% strain, and a heat rate of 0.5°C/min on 5, 10, 20, and 30% (w/w) $N_{95}BA_5$ samples.

Compression test

To perform compression testing, liquid hydrogels were injected into a 17-mm × 17-mm × 5-mm glass mold and then heated to 32°C using a temperature-controlled Instron 5567 mechanical tester. After a 2-min curing period, the glass mold was removed, and the probe was placed in contact with the top of the molded hydrogel. The samples were then compressed at a rate of 1 mm/min. A stress-strain curve was obtained, and compressive modulus was determined as the slope of the linear region corresponding to 5 to 15% strain. The number of hydrogel samples was three per group.

Tensile test

Liquid hydrogel samples were shifted to the solid phase (32°C) using a hot plate and were detached from a metal mold. Samples were then blotted dry and fixed by two clamps of an Instron 5942 mechanical tester. The solid samples were stretched at a constant rate of 1 mm/min under controlled temperature. Young's modulus was determined as the slope of the linear region of the stress-strain corresponding to 0 to 10% strain.

Hydrodynamic light scattering analysis

Intensity distribution and R_H of 5% (w/w) $N_{95}BA_5$ aggregates were measured by the automated DynaPro Plate Reader II (Wyatt Technology). The DLS equipment is equipped with a thermostat-equipped sample chamber to maintain desired temperatures within a range of 4° to 85°C with great accuracy. A bubble-free sample of about 80 μl was introduced in a square glass cuvette through a micropipette. A drop of mineral oil (20 μl) was placed on the top sample solution to prevent water evaporation. Then, the sample cell was placed in the sample chamber of the DLS instrument and kept at constant temperature for 30 min, a procedure repeated for all desired temperatures to ensure thermodynamic equilibrium. This instrument measures the movement of particles under Brownian motion and converts this motion into size by using the Stokes-Einstein equation, as given below,

$$D = kT/6\pi\eta R_H$$

where k is the Boltzmann's constant, T is the absolute temperature, η is the viscosity, and D is the diffusion coefficient. All data were obtained by the instrumental software.

Ex vivo IOP measurement

Fresh (harvested within 24 hours) porcine eyes (Sierra for Medical Science) were mounted into a Styrofoam fixture and immobilized with dissection pins. Partial core vitrectomies were performed on each eye using the Constellation Vision System vitrectomy console (Alcon Inc.), and

IOP was measured by a digital pressure sensor inserted in the vitreous cavity (posterior segment of the eye) (Fig. 3A). A single 3-mm linear incision was created in the sclera, about 3-mm distance radial from the limbus, with the incision path running tangential to the limbus perimeter. An infusion cannula was placed in the vitreous cavity on the opposite side from the incision to supply a saline solution of about 37°C. Saline solution was infused either from a gravity-fed saline drip bag or from a digitally actuated infusion system. Partial core vitrectomy allowed faster diffusion of the liquid through the vitreous cavity, and saline ejection from the incision site confirmed incision success. Once confirmed, the infusion line was clamped to limit leakage during the test. The eye surface was dried with swabs to enable clean placement of the test substance (Fig. 3A). After this process, the IOP was gradually raised from baseline by manually increasing the infusion pump pressure until leakage was observed or the pressure sensor value no longer increased with increasing infusion rate (indicative of a nonvisible leak). The maximum pressure held (in millimeters of mercury) was recorded.

In vitro adhesion test

We prepared a range of 0.8 to 43% (w/w) PNIPAM and 30% (w/w) $N_{95}BA_5$ hydrogels for uniaxial adhesion testing. Fresh (harvested within 24 hours) porcine eyes (Sierra for Medical Science) were dissected into a 2-cm × 2-cm square shape. Hydrogel was compressed between two pieces of dissected scleral tissue fixated to the base and actuator arm of the pull tester (Fig. 3F). Apposed tissues were put into contact and pressed together using 15*g* of pressure for 2 min. The actuator then performed a pulling motion until the two samples separated, compromising the gel adhesion.

Deployment tool development and use

To deploy the hydrogel in the eye, a novel tool was developed as follows: an 18-gauge intravenous catheter tip trimmed to 5 to 8 mm was attached onto the Luer-Lock end of the 1-cm^3 syringe, which was inserted through the opening of the 15-cm^3 syringe. The space between the external wall of the 1-cm^3 syringe and the internal wall of the 15-cm^3 syringe was filled with ammonium nitrate and water. The endothermic dissolution reaction for the cooling mechanism was calibrated by using a pair of digital thermocouples to track the temperature in the jacketing chamber and inside the hydrogel chamber when different quantities of water and ammonium nitrate were mixed together. A working range of about 7 to 15 ml of water mixed with 6 to 8 g of ammonium nitrate would result in a temperature-lowering profile meeting the performance criteria. For testing and use, the tool components were first sterilized, and then, a sterile 1-cm^3 syringe loaded with hydrogel was loaded into the jacket. The jacket was loaded with ammonium nitrate and capped with a rubber vial cap. When ready for use, a separate syringe filled with sterile water and capped with an 18-gauge needle was inserted through the rubber vial cap, and water was injected into the jacket chamber. The tool was shaken a few times vigorously to initiate the reaction. After 60 s, the gel was ready for application.

Hydrogel preparation for in vivo validation

The 30% $N_{95}BA_5$ hydrogel used for in vivo characterization was sterilized by first measuring a prescribed quantity (1.0 g) of the dried powder form into a 10-cm^3 glass crimp vial container. Each open and filled container was placed inside a Tyvek sterilization pouch with the associated stopper and crimp top. The pouch was then sealed and ethylene oxide–sterilized. Still inside the sealed and sterilized pouch, the stopper and crimp top were manipulated on top of the open container, and the container was crimped shut inside the pouch. Once sealed, the pouch was opened, and the jar was withdrawn, leaving a sealed crimp container with 0.5 g of sterile hydrogel powder. The sterilized hydrogel powders were hydrated by injecting sterile water into the vial and performing the hydration procedure described previously. Once hydrated, the containers were transferred to a refrigerator for storage until use.

In vivo study design

An unblinded, two-arm randomized (2:1, treatment/control) study was conducted, in which all animals received 3-mm full-thickness incisions in the sclera of the right eye (OS) about 3 mm posterior to the limbus in the temporal superior quadrant to mimic a traumatic injury. The fellow eye (OD) in all rabbits was left untouched as a control. Treatment group animals received the hydrogel intervention. Control group animals received no intervention (current standard of care). Pigmented New Zealand rabbits were used for this study because the eye dimensions closely approximate the size of the human eye, thus mimicking approximate conditions for human use of the system.

For treatment group rabbits, once the open globe injury was created, the hydrogel-loaded syringe was prepared for use, as described previously. About 0.1 to 0.3 cm^3 of hydrogel was used for each procedure. Control group rabbits received the same surgical procedure to the right eye but received no intervention. At the end of each procedure, all rabbits in both groups received (quantity) subcutaneous injections of buprenorphine with repeat injections at 12-hour intervals for 48 hours. The research team regularly monitored each rabbit for the first 6 hours after the procedure. They then performed checkups at 6-hour intervals through the first 12 hours, followed by 12-hour interval checkups through the first week. At each 12-hour follow-up, rabbits were removed from their cage, and their eyes were visually inspected by the research team for any evidence of adverse tissue responses, such as swelling, inflammation, or bleeding from the sclera, conjunctiva, or other surrounding tissues, with instructions to notify the ophthalmologists of the team of any adverse events.

In vivo IOP measurements

IOP of both eyes of all animals was measured using a magnetically actuated veterinary rebound tonometer (Tonovet). Baseline IOP values were established by measuring IOP of each eye twice daily (a.m. and p.m.) for 5 days leading up to the procedure (Fig. 5D). The Tonovet calculates an average reading from six tonometric measurements taken in succession. Four successive readings were taken on each eye; thus, 24 measures contributed to the averaged IOP for each eye. For all tonometry measures, rabbits were removed from the cage and placed on an evaluation table for 2 min to allow the animal to relax. Stress from handling is known to artificially elevate blood pressure and IOP values. The average of three IOP measurements was recorded at each time point for each eye (both OS and OD) at regular intervals after the surgical procedure. Normalized IOP values were reported by dividing IOP_{OS} by IOP_{OD} to reduce the impact of confounding systemic effects (stress, infection, and medications). All surgical procedures were performed in the a.m. and completed before noon, thus allowing IOP measures to resume in the late p.m. of the same day.

In vivo study endpoint

Study endpoints for the rabbits were set at 48 hours, 1 week, and 4 weeks to evaluate the progression of the tissue response at the implant site. Rabbits were not followed longer than 4 weeks because the intended use of the hydrogel will be for less than 30 days. Rabbits were euthanized

by first administering a heavy dose of ketamine/xylazine anesthesia, followed by intravenous injection of a lethal dose of sodium pentobarbital via the auricular vein. Once euthanized, a surgical procedure was performed to quickly enucleate and fix the study eyes (OS).

In vivo histology analysis

Enucleated eyes were fixed in Davidson's solution to preserve structure of the total globe. Tissues were sectioned and stained with either hematoxylin and eosin (H&E) or Masson's trichrome stain to evaluate local inflammatory response and characterize fibrosis. Retinal detachments were assessed by histological evaluation of the posterior segments at study endpoints. Retinas were analyzed for evidence of photoreceptor outer segment disorganization or complete degeneration, indicative of retina separation from the choroidal vasculature and nutrient supply. In addition to evaluation of the overall structure, tissues were sent to an outside pathology laboratory (Comparative Bioscience Inc.) to be evaluated by a certified veterinary pathologist for evidence of cytotoxic or neurotoxic effects of the hydrogel on surrounding tissues.

Statistical analysis

For each animal at each time point, a normalized IOP measurement was calculated as IOP_{OD}/IOP_{OS} (Fig. 5E). The normalized measurement was statistically compared between treated and untreated groups using a generalized estimating equations model to account for correlated data arising from the repeated measures of IOP within an animal. The repeatedly measured normalized IOP was the dependent variable; independent variables were treatment group and time (day, a.m./p.m.) of measurement. The postsurgery treatment effect on IOP was tested over all postsurgical assessments, as well as at each measurement time. An omnibus test of treatment effect over postinjury time was tested by a score test of the main effect of treatment. Time-specific treatment effects were compared between groups with the addition of a day-by-treatment interaction term; treatment group differences were compared at each time point with a Wald test looking for a statistically significant difference between the two groups ($\alpha = 0.05$; two-sided). Mean (Standard Error of the Mean, SEM) outcome measurements were estimated and plotted for each day and treatment group. Eighteen animals randomized in a 2:1 fashion provided exceptional power (>95% for the treatment effect throughout follow-up time) to evaluate the mean group differences observed.

SUPPLEMENTARY MATERIALS

www.sciencetranslationalmedicine.org/cgi/content/full/9/419/eaan3879/DC1

Materials and Methods

Fig. S1. Schematic synthesis routes of the $N_{85}NT_{15}$ and $N_{95}BA_5$ copolymers.

Fig. S2. ^1H NMR spectrum for $N_{85}NT_{15}$ and $N_{95}BA_5$ copolymers in $CDCl_3$.

Fig. S3. Scattering intensity spectra of $N_{95}BA_5$ as a function of temperature.

Fig. S4. Strain amplitude for $N_{95}BA_5$ and $N_{85}NT_{15}$ at $T = 6$°C.

Fig. S5. Strain amplitude of $N_{85}NT_{15}$ at its LCST.

Fig. S6. Complex viscosity of $N_{95}BA_5$ as a function of temperature and concentration.

Fig. S7. Compressive stress-strain characterization and compressive modulus of the $N_{95}BA_5$ hydrogel.

Fig. S8. Tensile stress-strain characterization and tensile modulus of the $N_{95}BA_5$ hydrogel.

Fig. S9. Intensity distribution graph of DLS spectra for $N_{95}BA_5$ recorded at different temperatures.

Fig. S10. Hydrophobic/hydrophilic nature of the $N_{95}BA_5$ hydrogel above and below the LCST.

Fig. S11. Injector tool cooling reaction calibration curves for 2.5 and 12.5 g of ammonium nitrate to various volumes of added water.

Fig. S12. Visual evaluation of eye responses to surgical procedure and sealant placement.

Fig. S13. TRS in the hands of professionals: In vitro application at Walter Reed Medical Center.

Table S1. Injector tool design requirements.

Table S2. In vivo study tabulated trajectory.

Table S3. In vivo statistical analysis of average OD/OS for groups over time.

Table S4. Scleral tissue response at the hydrogel-sclera interface.

Table S5. Responses from freehand write-in section of user survey administered during clinical user workshop.

Table S6. Responses from multiple choice section of user survey administered during clinical user workshop.

Movie S1. In vivo trauma simulation and hydrogel application procedure.

REFERENCES AND NOTES

1. G. McGwin Jr., T. A. Hall, A. Xie, C. Owsley, Trends in eye injury in the United States, 1992–2001. *Invest. Opthalmol. Vis. Sci.* **47**, 521–527 (2006).
2. F. Kuhn, D. J. Pieramici, Eds., *Ocular Trauma: Principles and Practice* (Thieme, 2002), 498 pp.
3. D. L. Cruvinel Isaac, V. C. Ghanem, M. A. Nascimento, M. Torigoe, N. Kara-José, Prognostic factors in open globe injuries. *Ophthalmologica* **217**, 431–435 (2003).
4. A. A. Honeycutt, S. D. Grosse, L. J. Dunlap, D. E. Schendel, H. Chen, E. Brann, G. al Homsi, Economic costs of mental retardation, cerebral palsy, hearing loss, and vision impairment, in *Using Survey Data to Study Disability: Results from the National Health Interview Survey on Disability*, B. M. Altman, S. N. Barnartt, G. E. Hendershot, S. L. Larson, Eds. (Elsevier, 2003), pp. 207–228.
5. R. J. Blanch, R. A. H. Scott, Military ocular injury: Presentation, assessment and management. *J. R. Army Med. Corps* **155**, 279–284 (2009).
6. G. A. Byrnes, Primary repair of the posterior segment: Penetrating, perforating, and blunt rupture injuries, in *Ophthalmic Care of the Combat Casualty,* A. B. Thach, Ed. (Office of the Surgeon General at TMM Publications, 2003), chap. 13, pp. 211–223.
7. Y. Yonekawa, H. D. Hacker, R. E. Lehman, C. J. Beal, P. B. Veldman, N. M. Vyas, A. S. Shah, D. Wu, D. Eliott, M. F. Gardiner, M. C. Kuperwaser, R. H. Rosa Jr., J. E. Ramsey, J. W. Miller, R. A. Mazzoli, M. G. Lawrence, J. G. Arroyo, Ocular blast injuries in mass-casualty incidents: The marathon bombing in Boston, Massachusetts, and the fertilizer plant explosion in West, Texas. *Ophthalmology* **121**, 1670–1676 (2014).
8. F. G. La Piana, T. H. Mader, Lessons learned, in *Ophthalmic Care of the Combat Casualty,* A. B. Thach, Ed. (Office of the Surgeon General at TMM Publications, 2003), chap. 2, pp. 17–39.
9. G. Koranyi, S. Seregard, E. D. Kopp, Cut and paste: A no suture, small incision approach to pterygium surgery. *Brit. J. Ophthalmol.* **88**, 911–914 (2004).
10. R. C. Hall, A. J. Logan, A. P. Wells, Comparison of fibrin glue with sutures for pterygium excision surgery with conjunctival autografts. *Clin. Exp. Opthalmol.* **37**, 584–589 (2009).
11. B. J. Vote, M. J. Elder, Cyanoacrylate glue for corneal perforations: A description of a surgical technique and a review of the literature. *Clin. Exp. Opthalmol.* **28**, 437–442 (2000).
12. M. Forseth, K. O'Grady, D. M. Toriumi, The current status of cyanoacrylate and fibrin tissue adhesives. *J. Long Term Eff. Med. Implants* **2**, 221–233 (1992).
13. G. Chen, A. S. Hoffman, Graft copolymers that exhibit temperature-induced phase-transitions over a wide range of pH. *Nature* **373**, 49–52 (1995).
14. A. S. Hoffman, Environmentally sensitive polymers and hydrogels. *MRS Bull.* **16**, 42–46 (1991).
15. M. A. Cole, N. H. Voelcker, H. Thissen, H. J. Griesser, Stimuli-responsive interfaces and systems for the control of protein–surface and cell–surface interactions. *Biomaterials* **30**, 1827–1850 (2009).
16. A. Halperin, M. Kröger, F. M. Winnik, Poly(*N*-isopropylacrylamide) phase diagrams: Fifty years of research. **54**, 15342–15367 (2015).
17. S. Shekhar, M. Mukherjee, A. K. Sen, Swelling, thermal and mechanical properties of NIPAM-based terpolymeric hydrogel. *Polym. Bull.* **73**, 125–145 (2016).
18. L. T. Allen, E. J. P. Fox, I. Blute, Z. D. Kelly, Y. Rochev, A. K. Keenan, K. A. Dawson, W. M. Gallagher, Interaction of soft condensed materials with living cells: Phenotype/transcriptome correlations for the hydrophobic effect. *Proc. Natl. Acad. Sci. U.S.A.* **100**, 6331–6336 (2003).
19. W.-F. Lee, Y.-C. Yeh, Studies on preparation and properties of NIPAAm/hydrophobic monomer copolymeric hydrogels. *Eur. Polym. J.* **41**, 2488–2495 (2005).
20. E. Velzenberger, K. El Kirat, G. Legeay, M.-D. Nagel, I. Pezron, Characterization of biomaterials polar interactions in physiological conditions using liquid–liquid contact angle measurements: Relation to fibronectin adsorption. *Colloids Surf. B Biointerfaces* **68**, 238–244 (2009).
21. Q. Wang, J. L. Mynar, M. Yoshida, E. Lee, M. Lee, K. Okuro, K. Kinbara, T. Aida, High-water-content mouldable hydrogels by mixing clay and a dendritic molecular binder. *Nature* **463**, 339–343 (2010).
22. M. Banitt, J. B. Malta, H. K. Soong, D. C. Musch, S. I. Mian, Wound integrity of clear corneal incisions closed with fibrin and N-butyl-2-cyanoacrylate adhesives. *Curr. Eye Res.* **34**, 706–710 (2009).
23. K. A. Vakalopoulos, Z. Wu, L. Kroese, G.-J. Kleinrensink, J. Jeekel, R. Vendamme, D. Dodou, J. F. Lange, Mechanical strength and rheological properties of tissue adhesives with regard to colorectal anastomosis: An ex vivo study. *Ann. Surg.* **261**, 323–331 (2015).
24. R. Shaikh, T. Raj Singh, M. Garland, A. Woolfson, R. F. Donnelly, Mucoadhesive drug delivery systems. *J. Pharm. Bioall. Sci.* **3**, 89–100 (2011).

25. B. Natalia, A. Henry, L. Betty, R. L. Marina, R. Roberto, Probing poly(*N*-isopropylacrylamide-*co*-butylacrylate)/cell interactions by atomic force microscopy. *J. Biomed. Mater. Res. A* **103**, 145–153 (2015).
26. P. M. Reddy, P. Venkatesu, Ionic liquid modifies the lower critical solution temperature (LCST) of poly(*N*-isopropylacrylamide) in aqueous solution. *J. Phys. Chem. B* **115**, 4752–4757 (2011).
27. J. W. McLaren, R. F. Brubaker, J. S. FitzSimon, Continuous measurement of intraocular pressure in rabbits by telemetry. *Invest. Ophthalmol. Vis. Sci.* **37**, 966–975 (1996).
28. F. H. Adler, R. A. Moses, W. M. Hart, *Adler's Physiology of the Eye: Clinical Application* (Mosby, 1987).
29. J. M. Anderson, A. Rodriguez, D. T. Chang, Foreign body reaction to biomaterials. *Semin. Immunol.* **20**, 86–100 (2008).
30. D. W. Herr, W. K. Boyes, Electrophysiological analysis of complex brain systems: Sensory-evoked potentials and their generators, in *Neurotoxicology: Approaches and Methods*, L. W. Chang, W. Slikker Jr., Eds. (Academic Press, 1995), chap. 9, pp. 208–221.
31. D. A. X. Nayagam, C. McGowan, J. Villalobos, R. A. Williams, C. Salinas-LaRosa, P. McKelvie, I. Lo, M. Basa, J. Tan, C. E. Williams, Techniques for processing eyes implanted with a retinal prosthesis for localized histopathological analysis. *J. Vis. Exp.* **78**, e50411 (2013).
32. A. Gutowska, Y. H. Bae, H. Jacobs, F. Mohammad, D. Mix, J. Feijen, S. W. Kim, Heparin release from thermosensitive polymer coatings: In vivo studies. *J. Biomed. Mater. Res.* **29**, 811–821 (1995).
33. P. N. Wahjudi, J. H. Oh, S. O. Salman, J. A. Seabold, D. C. Rodger, Y.-C. Tai, M. E. Thompson, Improvement of metal and tissue adhesion on surface-modified parylene C. *J. Biomed. Mater. Res. A* **89**, 206–214 (2009).
34. B. Brugger, J. Vermant, W. Richtering, Interfacial layers of stimuli-responsive poly-(*N*-isopropylacrylamide-*co*-methacrylicacid) (PNIPAM-*co*-MAA) microgels characterized by interfacial rheology and compression isotherms. *Phys. Chem. Chem. Phys.* **12**, 14573–14578 (2010).
35. A. C. Kumar, H. B. Bohidar, A. K. Mishra, The effect of sodium cholate aggregates on thermoreversible gelation of PNIPAM. *Colloids Surf. B Biointerfaces* **70**, 60–67 (2009).
36. A. C. Kumar, H. Erothu, H. B. Bohidar, A. K. Mishra, Bile-salt-induced aggregation of poly(*N*-isopropylacrylamide) and lowering of the lower critical solution temperature in aqueous solutions. *J. Phys. Chem. B* **115**, 433–439 (2011).
37. C. Monteux, R. Mangeret, G. Laibe, E. Freyssingeas, V. Bergeron, G. Fuller, Shear surface rheology of poly(*N*-isopropylacrylamide) adsorbed layers at the air–water interface. *Macromolecules* **39**, 3408–3414 (2006).
38. S. Kaja, D. L. Goad, F. Ali, A. Abraham, R. L. Rebenitsch, S. Teymoorian, R. Krishna, P. Koulen, Evaluation of tensile strength of tissue adhesives and sutures for clear corneal incisions using porcine and bovine eyes, with a novel standardized testing platform. *Clin. Opthalmol.* **6**, 305–309 (2012).
39. R. Mentens, Comparison of fibrin glue and sutures for conjunctival closure in pars plana vitrectomy. *Am. J. Ophthalmol.* **144**, 128–131 (2007).
40. M. Rahimi, S. Kilaru, G. E. Sleiman, A. Saleh, D. Rudkevich, K. Nguyen, Synthesis and characterization of thermo-sensitive nanoparticles for drug delivery applications. *J. Biomed. Nanotechnol.* **4**, 482–490 (2008).
41. Z. Cui, B. H. Lee, C. Pauken, B. L. Vernon, Degradation, cytotoxicity, and biocompatibility of NIPAAm-based thermosensitive, injectable, and bioresorbable polymer hydrogels. *J. Biomed. Mater. Res. A* **98A**, 159–166 (2011).
42. F. A. Andersen, Amended final report on the safety assessment of polyacrylamide and acrylamide residues in cosmetics. *Int. J. Toxicol.* **24** (suppl. 2), 21–50 (2005).
43. R. Zhu, G. Wu, X. Liu, D. Shi, B. Cao, R. Gu, J. Xiao, H. Liao, PNIPAM hydrogel induces skeletal muscle inflammation response. *RSC Adv.* **5**, 28023–28029 (2015).
44. L. Zou, A. Nair, H. Weng, Y.-T. Tsai, Z. Hu, L. Tang, Intraocular pressure changes: An important determinant of the biocompatibility of intravitreous implants. *PLOS ONE* **6**, e28720 (2011).
45. N. Y. Becerra, B. L. López, L. M. Restrepo, Thermosensitive behavior in cell culture media and cytocompatibility of a novel copolymer: Poly(*N*-isopropylacrylamide-*co*-butylacrylate). *J. Mater. Sci. Mater. Med.* **24**, 1043–1052 (2013).

Acknowledgments: We acknowledge W. Mack from the Biostatistics group at the USC Clinical and Translational Sciences Institute (SC-CTSI) for the statistical analyses performed and reported in this paper. We further acknowledge J. Cortez for contributions to the design and testing of the injector tool described and used in this study. We thank S. Nutt, M. McCain, Y. Zhang, and D. Leite for assistance with the operation of Instron mechanical testers described herein. We thank D. Sylvinson for help with the graphic illustrating the polymer structure, which was generated using Schrodinger's Materials Science Suite. **Funding:** This work was supported by funding from the Office of the Assistant Secretary of Defense for Health Affairs through the FY12 Vision Research Program under award no. W81XWH12-1-0314, the NIH through the SC-CTSI program [NIH/National Center for Research Resources (NCRR)/ National Center for Advancing Translational Science (NCATS)] through grants UL1TR000130 and UL1TR001855 from NCATS, the NSF through award EEC-0310723, and an unrestricted departmental grant from Research to Prevent Blindness. Note that the opinions, interpretations, conclusions, and recommendations presented here are those of the authors and are not necessarily endorsed by or representative of the official views of the U.S. Department of Defense, NIH, or Research to Prevent Blindness Foundation. **Author contributions:** N.B., J.J.W., and M.E.T. designed the research. N.B. contributed to all the facets of this work's development; fabricated hydrogel compositions and oversaw the initial copolymer design; designed and performed characterization studies of the material properties, including but not limited to NMR, light scattering, DLS, and mechanical analysis; facilitated data procurement during ex vivo benchtop measures and provided procedural support during the in vivo studies; and provided a major contribution to this article through a significant portion of the text and design of all figures. Y.Z. designed both ex vivo benchtop testing platforms (uniaxial test and IOP infusion test) used for characterizing the performance characteristics of the hydrogel on tissues; produced, loaded, and sterilized the injector tools for the in vivo studies; provided general support for the in vivo study design, setup, and execution; and performed all in vivo IOP measurements and tracked the daily health of all animals. Y.Z. also helped with compiling histology samples for the study. P.F. provided early clinical user feedback on system design; performed the in vivo implantation tests and the follow-up evaluations, euthanization, and eye enucleations for histology; and provided clinical insights into the interpretation of the results and guidance on writing this manuscript. R.M. aided in the hydrogel solution preparation; performed characterization studies of hydrogel material properties, including rheology, DLS, and mechanical analysis; and provided major written contribution to the final work. J.J.W. wrote the original protocols and study designs for the ex vivo and in vivo performance testing; coordinated the histology preparation; collected and compiled histology data; wrote most of the in vivo data sections and their interpretation, as well as the ex vivo data interpretation; project-managed the program; and was a co-investigator on the award funding this project. M.S.H. provided clinical and biomedical engineering guidance on the overall strategy for this project, provided clinical interpretation of the results, performed a final revision of this manuscript, and is the principal investigator of the award that funded the work presented here. M.E.T. provided guidance and insight into the polymer chemistry synthesis, composition, and materials characterization approaches; provided interpretation of the results regarding the polymer chemistries used; performed a final revision of this paper; and was a co-investigator on the award funding this project. **Competing interests:** J.J.W., N.B., Y.Z., P.F., M.E.T. and M.S.H. are inventors on patent application 15/013,632 submitted by the University of Southern California that covers the entire ocular trauma intervention system presented here, including both the hydrogel materials and the injector tool. R.M. declares that he has no competing interests. **Data and materials availability:** The data sets, materials, and analysis generated during the current study are available from the corresponding author on reasonable request.

Submitted 5 April 2017
Resubmitted 2 August 2017
Accepted 23 October 2017
Published 6 December 2017
10.1126/scitranslmed.aan3879

Citation: N. Bayat, Y. Zhang, P. Falabella, R. Menefee, J. J. Whalen, M. S. Humayun, M. E. Thompson, A reversible thermoresponsive sealant for temporary closure of ocular trauma. *Sci. Transl. Med.* **9**, eaan3879 (2017).

Science Translational Medicine

A reversible thermoresponsive sealant for temporary closure of ocular trauma

Niki Bayat, Yi Zhang, Paulo Falabella, Roby Menefee, John J. Whalen III, Mark S. Humayun and Mark E. Thompson

Sci Transl Med **9**, eaan3879.
DOI: 10.1126/scitranslmed.aan3879

A sealant to save sight

Traumatic eye injuries require rapid treatment to prevent deterioration of vision. As an alternative to suturing or adhesives, Bayat and colleagues developed a temperature-responsive synthetic hydrogel that acts as a temporary sealant. Testing the hydrogel in a model of open globe injury in rabbits showed that the sealant was easily deployed from a custom-designed temperature-controlled syringe device and preserved intraocular pressure without evidence of chronic inflammation or toxicity. After gelation, the sealant could be removed by exposure to cold water. In combat or low-resource settings, this hydrogel could close wounds temporarily to prevent further tissue damage or vision loss before surgery.